Tuning Structural and Optical Properties of Copper Oxide Nanomaterials by Thermal Heating and Its Effect on Photocatalytic Degradation of Congo Red Dye

Rehman, Sidra
Department of Physics, University of Agriculture Faisalabad, 38000, Faisalabad, PAKISTAN

Akhtar Shad, Naveed
Department of Physics, Government College University Faisalabad, Faisalabad, PAKISTAN

Munir Sajid, Muhammad
Henan Key Laboratory of Photovoltaic Materials, School of Physics, Henan Normal University, Xinxiang 453007, P.R. CHINA

Ali, Khuram; Javed, Yasir*[+]; Jamil, Yasir; Sajjad, Muhammad; Nawaz, Ahmad
Department of Physics, University of Agriculture Faisalabad, 38000, Faisalabad, PAKISTAN

Kumar Sharma; Surender
Department of Physics, Central University of Punjab, Bathinda, INDIA

ABSTRACT: *In this study, Copper oxide (CuO) nanoparticles (NPs) were prepared using the chemical co-precipitation method and treated at different calcination temperatures. The synthesized CuO NPs have been calcinated at 300 °C, 500 °C, and 700 °C. The X-Ray Diffraction (XRD) results exhibited a decrease in the width of the principle diffraction peak with the temperature rise. Crystallite size was determined by Scherrer's formula, whereas, the Williamson-Hall method presented drastic variation in size indicating the creation of lattice strain with the rise in calcination temperature. Scanning Electron Microscopy (SEM) images showed an increase in grain size and vary from 170 nm – 430 nm. X-ray Energy Dispersive Spectroscopy (EDS) results indicate the formation of CuO NPs and relative Cu contents increased (52.9 to 72.5 Atomic percentage) with temperature. Optical properties are also affected by the calcination temperature and a reduction in bandgap is observed with the increase in temperature. Fourier Transform Infra-Red (FT-IR) spectroscopy spectra of different samples showed identical bonding behavior and no apparent change in bonding was observed. Photo-degradation of Congo Red dye was performed with CuO NPs treated at different temperatures and NPs treated at 500 °C, have shown maximum degradation efficiency in 75 min under visible light.*

KEYWORDS: *Thermal effects; CuO NPs; Calcination; Bandgap tuning; Variant chemical composition; photocatalytic activity.*

***** *To whom correspondence should be addressed.*
+ E-mail: myasi60@hotmail.com
1021-9986/2022/5/1549-1560 12/$/6.02

INTRODUCTION

Nanomaterials have received attention owing to their large surface area, and quantum effect, and exhibited much improved characteristics as compared to bulk materials [1,2]. Nanomaterials are extensively studied for biological and optical sensors [3], coating formulations [4], photocatalysis [5-8], and photovoltaic cells [9]. However, there are still different challenges, such as shape control, size, size distribution, the release rate, and stability of nanoparticles (NPs), which need to be addressed [10,11]. During the last two decades, the scientific community and engineers are highly interested in metal oxide nanostructures due to their tremendous applications in various fields [12,13]. Among transition metal oxides, copper oxide (CuO) is a monoxide compound with p-type nature and a narrow bandgap (1.2 eV) semiconductor. Due to low electrical resistance, CuO NPs have been used as a heterogeneous catalyst in several chemical processes, such as nitrous oxide degradation, phenol, and hydrocarbon in supercritical water [13,14]. CuO NPs have also applications in optical switches [15], magnetic storage media [16], gas sensors [17], solar cells [18], active catalysts [19], and lithium-ion batteries [20] due to their photochemical and photoconductive characteristics.

CuO crystallizes in the monoclinic braves lattice with space and point group symmetry C2/c (No.15) and P2/m respectively. At the corners of the rectangular parallelogram, the copper atom is enveloped by four oxygen atoms to form chains by sharing the edges. Moreover, at the corners of the distorted tetrahedron, the oxygen atom is linked with four copper atoms. The chain traverses the crystal structure in the directions of [110] and [-110] [21]. In the [001] direction, chains alternate and in the [010] direction, each chain is stacked with a separation of about 2.7 Å [14]. Cu_2O is the 2nd most stable phase and has a cubic structure with a lattice constant 4.2696 Å and space group Pn-3m (No. 224) [22]. In this unit cell, the copper atom is coordinated with two oxygen atoms. Cu_4O_3 is a mixture of Cu(I)/Cu(II) oxide, 3rd most stable phase of CuO with 1.33 atomic ratio, belonging to tetragonal structure and space group $I4_1/amd$ [23].

The oxidation stability of metal oxide is very important when applied in high-energy applications because of the change in phase, size, and other parameters due to heating can affect the efficiency of the nanomaterials. Therefore, stability studies under heat are very important. CuO has applications in high-temperature reactions and efficacy will certainly be affected by temperature changes [24]. Literature is reported on the effect of heating on CuO thin films. *Johan et al* [25] investigated copper oxide thin films annealed between 200 to 400 °C and observed that at different annealing temperatures, the structure of thin films was changed. At 200 °C, thin films have a cuprite (Cu_2O) structure, mixed cuprite (Cu_2O) and tenorite (CuO) phases at 300 °C, while changed into pure tenorite phase at 400 °C. *Raship et al*. [26] demonstrated a dip-coating sol-gel method for the growth of CuO films on Si substrates. The effect of different temperatures on CuO films was studied. It was observed that increasing the annealing temperature results reduction in resistivity, grain size, and surface roughness.

Copper oxide nanostructures can be synthesized by various methods i.e. sonochemical [27], wet chemical route [28], co-precipitation method [29], pulse laser ablation [30], sol-gel method [31], and hydrothermal method [32]. Among these methods, the chemical The co-precipitation method is a facile way for high yield due to low cost, temperature, and low energy consumption. In this study, the key objective was to evaluate the effect of temperature on the structure, morphology, optical, and photocatalytic properties of CuO nanomaterials. Chemical co-precipitation was used to prepare CuO NPs and calcinated at 300 °C, 500 °C, and 700 °C. Different characterization tools such as XRD, SEM, EDS, UV-Vis spectroscopy, and FTIR were used to investigate prepared samples.

EXPERIMENTAL SECTION

Chemicals

During the experiment, all analytical-grade chemicals were used without any further purification. Copper chloride dihydrate ($CuCl_2.2H_2O$), Sodium hydroxide (NaOH), and distilled water was used for preparing the CuO NPs.

Synthesis procedure

A standard procedure was adopted to synthesize CuO NPs [33]. During synthesis, firstly 0.3 M of $CuCl_2.2H_2O$ and 0.6 M of NaOH were dissolved in distilled water to prepare precursor solutions. At room temperature, NaOH was incorporated gradually into the solution of $CuCl_2.2H_2O$ under constant stirring. The solution color

was gradually changed from green to bluish-green and finally black while the reaction proceeded. The pH 11 was maintained throughout the reaction. Black precipitates were filtered and washed several times with distilled water to eliminate impurities. After that, precipitates were dried in the oven at 70 °C for 12 h. Dried samples were calcinated in the furnace at 300 °C, 500 °C, and 700 °C temperature for 2 h. The obtained samples were characterized by XRD, SEM, EDS, UV-Vis spectroscopy, and FT-IR. The overall chemical reaction can be expressed as:

$$CuCl_2 + 2NaOH \rightarrow CuO + 2NaCl + H_2O \quad (1)$$

Photocatalytic experiment

CuO NPs have been utilized for the degradation of Congo Red (CR) dye under visible light irradiation. First, a dye solution of 0.01 g/L was prepared and 0.1 g/L catalysts were inserted in the dye solution in the presence of a small amount of H_2O_2 and irradiated under visible light and the readings were noted every 15 min. Samples with different CuO (0.01, 0.05, 0.1, 0.2, 0.4 g/L) and dye (10, 15, 20, 25, 30 mg/L) concentrations have been prepared and evaluated. Prior to irradiation, the suspensions were stirred for 40 min in the dark to ensure the system attained the adsorption-desorption equilibrium. The prepared solutions were kept under visible light for 75 mins under ambient conditions. A Xenon lamp of 300 W was used as the visible light source. The final dye color has been investigated by taking absorption spectra using a UV-Vis spectrophotometer.

RESULTS AND DISCUSSION

Fig. 2: XRD spectra of CuO nanomaterials treated at different calcination temperatures, (a) The as-synthesized, (b) 300 °C, (c) 500 °C, (d) 700 °C, (e) Variation in peak broadening with temperature for the principle diffraction peak at the peak position 38.90°.

The XRD patterns of copper oxide samples treated at different temperatures are shown in Fig. 2(a-d). The diffraction peaks of as-synthesized, treated at 300 °C and 500 °C are well-matched with JCPDS card 00-041-0254, whereas, treated at 700 °C are matched with 00-041-0937 of copper oxide having a monoclinic crystal structure with C2/c space group. The position of the XRD peaks is consistent with CuO and high-intense sharp peaks indicate the crystalline nature. The peaks are observed at 32.53°, 35.63°, 38.90°, 48.45°, 53.84°, 58.38°, 61.69°, 66.00°, 68.15°, 72.33° and 75.15° corresponds to (110), (002), (200), (-202), (020), (202), (-113), (-311), (220), (311) and (004) diffraction planes respectively. In the XRD spectrum of copper oxide treated at 700 °C (Fig. 2d), an additional peak is observed at 46.16° belonging to the (-112) plane. No impurity peaks are detected in the XRD pattern which exhibits that CuO is well crystalline and pure. Fig. 2e shows the effect of calcination temperature on the peak broadening for the highest intensity diffraction peak. The peak width decreases with the temperature which indicates an improvement in the degree of crystallinity of the material.

XRD patterns of CuO nanomaterials are also used to calculate various crystal structure parameters. The lattice constants can be calculated by the following formula

$$\frac{1}{d^2} = \frac{1}{\sin^2\beta}\left(\frac{h^2}{a^2} + \frac{k^2\sin^2\beta}{b^2} + \frac{l^2}{c^2} + \frac{2hl\cos\beta}{ac}\right) \quad (2)$$

Where *d* is interatomic spacing, *a*, *b*, *c* are lattice constants. β is the angle of the monoclinic structure and is taken as 99.52°.

The volume of the unit cell of the monoclinic structure can also be calculated from the following formula:

$$V = abc\sin\beta \quad (3)$$

The packing factor can be found using the following formula,

$$\text{Atomic Packing Fraction} = \frac{\pi a^2}{6bc\sin\beta} \quad (4)$$

'a, b and *c*' is the lattice constant of monoclinic structure and β is an angle.

The density of the monoclinic unit cell can be calculated.

$$\rho = \frac{nM_W}{vN_A} \quad (5)$$

Where *n* is the number of atoms per unit cell, M_w is the molecular weight, *V* is the volume of the unit cell and N_A is Avogadro's number.

For a monoclinic structure, the value of 'n' is 4 because the unit cell has 4 atoms and accommodates four CuO dimers in the crystallographic unit cell and two CuO units in the primitive cell. Each copper atom is present in the center of an oxygen parallelogram [31]. M_w is taken

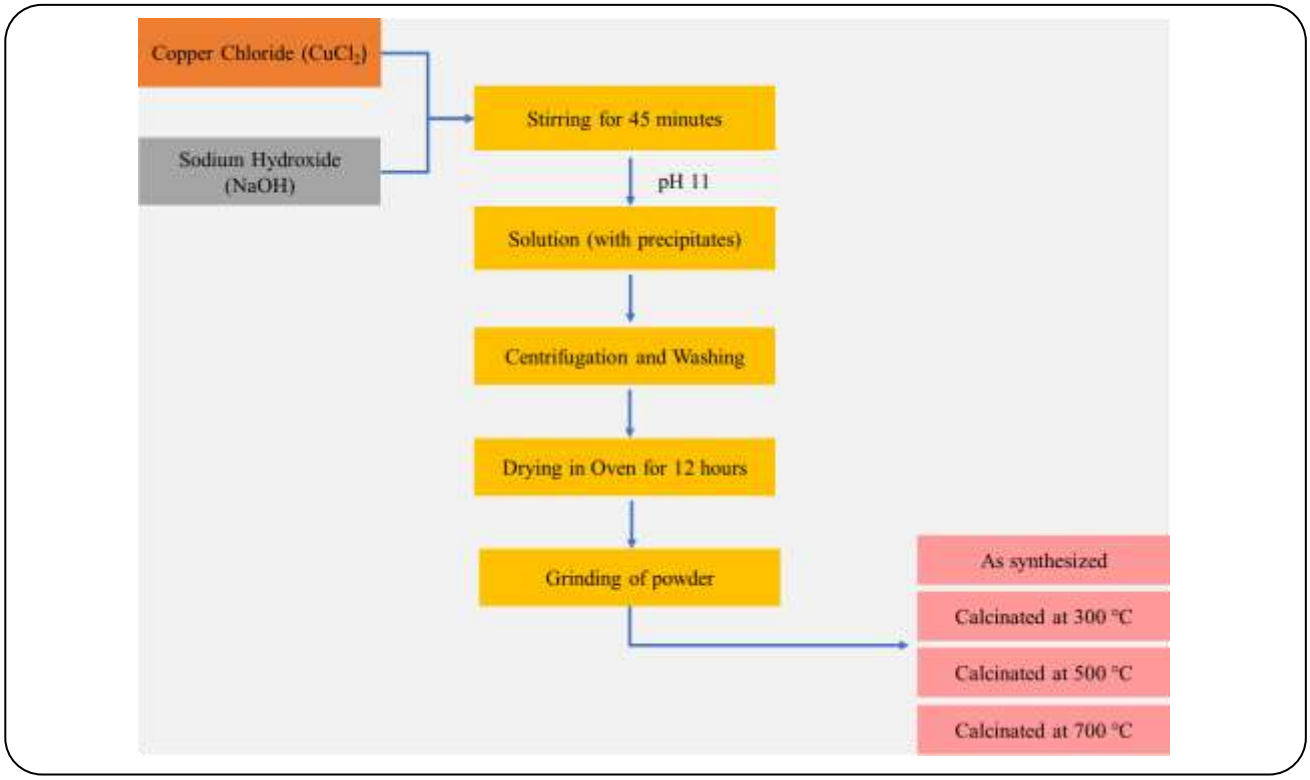

Fig. 1: Schematic representation of different steps involved in CuO nanomaterials.

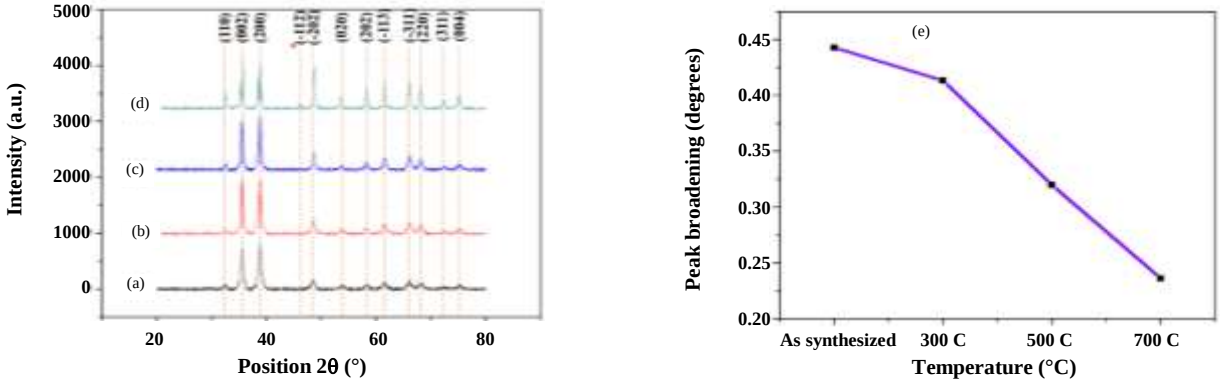

Fig. 2: XRD spectra of CuO nanomaterials treated at different calcination temperatures, (a) The as-synthesized, (b) 300 °C, (c) 500 °C, (d) 700 °C, (e) Variation in peak broadening with temperature for the principle diffraction peak at the peak position 38.90°.

as 79.54 g/mol. Values calculated for different parameters are presented in Table 1. There is an increase in lattice constant values observed for different temperatures, as a result, affected the volume of the unit cell. This increase explains the unit cell stretching which consequently affects the unit cell volume, packing fraction, and unit cell density.

Another parameter that can be calculated from the XRD pattern is the average crystallite size. Scherrer's formula is usually used to calculate the crystallite size with the formula given below,

$$D = 0.94\lambda/\beta\text{Cos}\theta \quad (6)$$

Where λ is the wavelength of X-rays, β is the full width at half maximum, θ is Bragg's angle and D is the crystalline average size [24]. Scherrer's formula has generally underestimated the value of crystallite size due to the absence of lattice strain in its relation. Therefore,

Table 1: Calculated values of lattice constants, unit cell volume, packing factor, and density.

Sample	Temperature (°C)	Lattice constant (Å)			Volume (Å^3)	APF	Density (g/cm^3)
		a	b	c			
Ref file	--	4.685	3.423	5.132	81.17	0.6629	6.51
1	As synthesized	4.694	3.405	5.109	80.5329	0.6721	6.56
2	300	4.699	3.414	5.1239	81.0675	0.6668	6.51
3	500	4.700	3.408	5.105	80.6437	0.6737	6.55
4	700	4.712	3.422	5.126	81.4611	0.7949	6.48

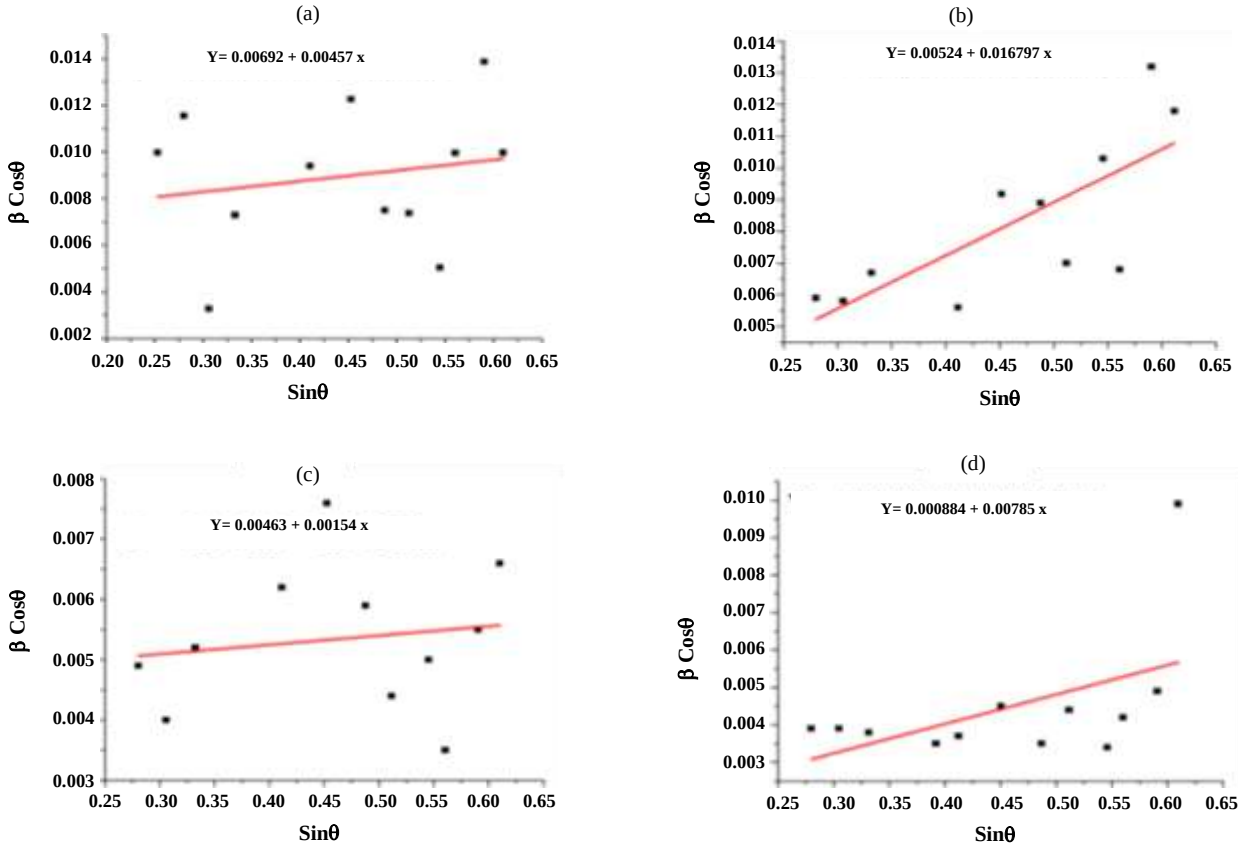

Fig. 3: W-H plots of XRD spectra of nanomaterials (a) as-synthesized, (b) 300 °C, (c) 500 °C, (d) 700 °C.

considering the strains present in the lattice due to crystal defects, Williamson-Hall (WH) method is a good approximation that considers and removes any broadening in the diffraction peaks due to lattice strains and instrumentation. The relation for WH method considering a uniform deformation model can be described as

$$\beta_{hkl}\text{Cos}\theta = \frac{K\lambda}{D} + 4\varepsilon\text{Sin}\theta \qquad (7)$$

Where D is crystallite size and ε is lattice strain. K is a constant with a value 0.94, β is peak broadening and the wavelength of X-rays is taken as 0.154 nm. A plot between Sinθ and βCosθ can be plotted and the equation of linear fit provides lattice strain and crystallite size. Fig. 3(a-d) shows WH plots of CuO powder treated at different temperatures. Linear fit equations are provided in Fig. 3. Table 2 shows a comparison of crystallite size calculated by Scherrer's formula and WH plots. The lattice strain calculated from the WH plot is also provided in Table 2. Crystallite size calculated by the Scherrer formula provided

Table 2: Effect of calcination temperature on average crystallite size D_{shr}, D_{wh}, and strain.

Temperature (°C)	D_{Shr} (nm)	D_{WH} (nm)	Strain
As-synthesized	18.81	20.92	0.00114
300 °C	23.78	276.25	0.04197
500 °C	28.05	31.26	0.00038
700 °C	32.7	163.75	0.00196

Table 3: Texture coefficients calculated for different samples.

Planes	As synthesized	300 °C	500 °C	Planes	700 °C
(110)	0.87400	0.9264	1.0030	(110)	1.1064
(002)	1.2743	1.6867	1.5350	(002)	0.8853
(200)	0.81120	1.1384	1.0313	(200)	1.023
(-202)	0.66145	0.9727	0.8902	(-112)	0.8851
(020)	0.7534	0.1124	0.7322	(-202)	1.082
(202)	0.6427	0.7722	0.888	(020)	0.8805
(-113)	0.71298	0.9655	0.87730	(202)	1.1311
(-311)	1.1661	1.17118	1.3057	(-113)	0.9286
(220)	2.6858	1.0107	0.943	(-311)	1.3053
(311)	0.5063	0.76847	0.6617	(220)	1.076
(004)	0.9178	0.8538	1.11324	(311)	0.6280
				(004)	1.0678

the expected trend of increase in size from 18.81 nm to 32.7 nm, but drastic changes are observed in crystallite size using WH method, were stresses in the lattice are considered. An increase in size is generally observed in the WH method which indicates that lattice strain is present in all the samples. When we talk specifically, from as-synthesized to 300 °C, size changes drastically from 20.92 nm to 276.25 nm indicating the creation of a large number of crystal defects with calcination temperature. At 500 °C, the crystallite size was reduced to 31.26 nm and rose, again at 700 °C, to 163.75 nm. Variations in the crystallite size of the two methods originated due to imperfections in the structure [34].

Another important parameter that can be deduced from the XRD pattern is the Texture Coefficient (T_C) which gives information about the preferred growth direction of the crystal. T_C can be calculated by the following formula

$$T_C = \frac{N(I/I_0)}{\sum(I/I_0)} \quad (8)$$

Where T_C is the coefficient texture, I and I_0 are relative intensities of synthesized and reference card patterns and N is the number of peaks matched with the reference card. The calculated values of texture coefficients for different CuO samples are provided in Table 3. The highest value of T_C in a given material indicates the preferred growth orientation of crystals during the growth process. From as synthesized to 500 °C, crystal growth is governed by [002] direction. T_C values vary for these three samples, however, indicate the same growth direction i.e. [002], whereas, for 700 °C, the preferred growth direction is [202].

SEM Analysis

The morphology of untreated and treated copper oxide nanomaterials is evaluated through scanning electron microscopy as shown in Fig. 4. SEM images of all the samples show that a high yield of nanomaterials is produced. Although it is observed that grain size is increased with the temperature rise, XRD showed

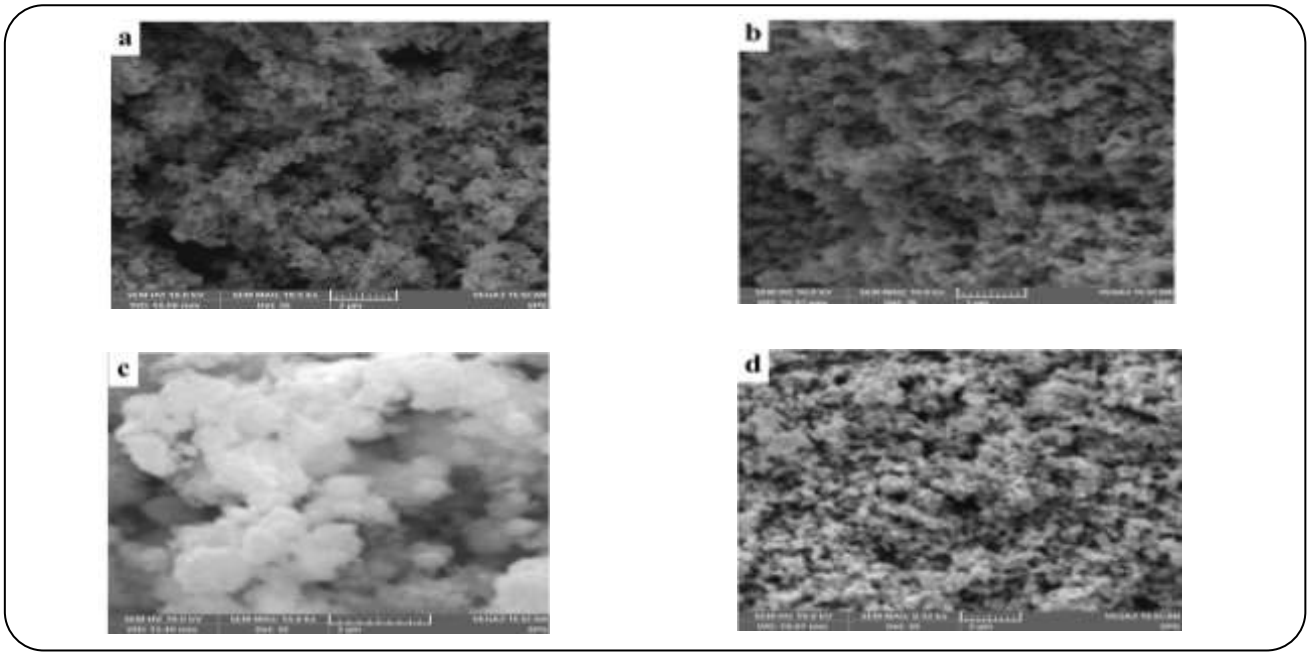

Fig. 4: SEM images of CuO nanomaterials calcinated at a different temperatures, (a) as-synthesized, (b) 300 °C, (c) 500 °C, (d) 700 °C.

that nanomaterial maintains its crystalline structure. The morphology of the nanostructure transforms during heating, as evident from the images at different temperatures. Initial morphology is irregular flake-like shapes observed till 300 °C. At 500 °C, flat surface types of large aggregates are observed, and with further increase in temperature i.e. 700 °C, fine particles with spherical morphology are witnessed. The SEM images show the non-uniform grains distributions in all compositions. The average grain size of CuO nanoparticles untreated, treated at 300 °C, 500 °C, and 700 °C are 170 nm, 220 nm, 430 nm, and 235 nm respectively. From these images, it can be observed that the calcinated NPs are more agglomerated and yet have a smooth surface as compared to untreated nanomaterials. The reason for agglomeration is the diffusion phenomenon and diffusion occurs due to the annealing of the material [35]. The particle aggregation rate is a prime influencer that controls the morphology and crystalline kinetics of the materials [36]. With the rise in calcination temperature, an increase in agglomeration is observed in SEM images. The increase in crystalline size and reduction in the surface area was also evidenced by the rise in calcination temperature in the literature [37].

EDS Analysis

Energy Dispersive Spectroscopy (EDS) has been used to detect changes in the chemical composition of the sample heated at different temperatures. Fig. 5(a-d) shows the EDS spectrum of CuO powder samples i.e. as synthesized, 300 °C, 500 °C, and 700 °C. The EDS spectrum displays only Cu and O peaks without any level of impurity, suggesting the synthesized nanomaterials are chemically pure. There is variation in relative atomic percentage (At %) with temperature, these changes may be linked with morphological changes that arise during heating. The spectra indicate the high chemical purity of the samples and the formation of CuO at the early stage of heating. The copper (Cu) and oxygen (O) compositions are increased due to the increase in temperature.

Optical Properties Analysis

UV-Visible absorption spectra of different copper oxide nanomaterials are shown in Fig. 6. A strong absorption peak in the visible region at 672 nm can be observed in all the samples. This absorption wavelength belongs to the bulk CuO material. The optical band gap is an important parameter to study the behavior of semiconductor materials as this provides an energy gap between valence and conduction bands. This is important to identify the efficiency of the synthesized nanomaterials and can be determined from the optical absorption spectrum of the material. The optical band gaps of all samples are evaluated by plotting Tauc's plot using Equation (8).

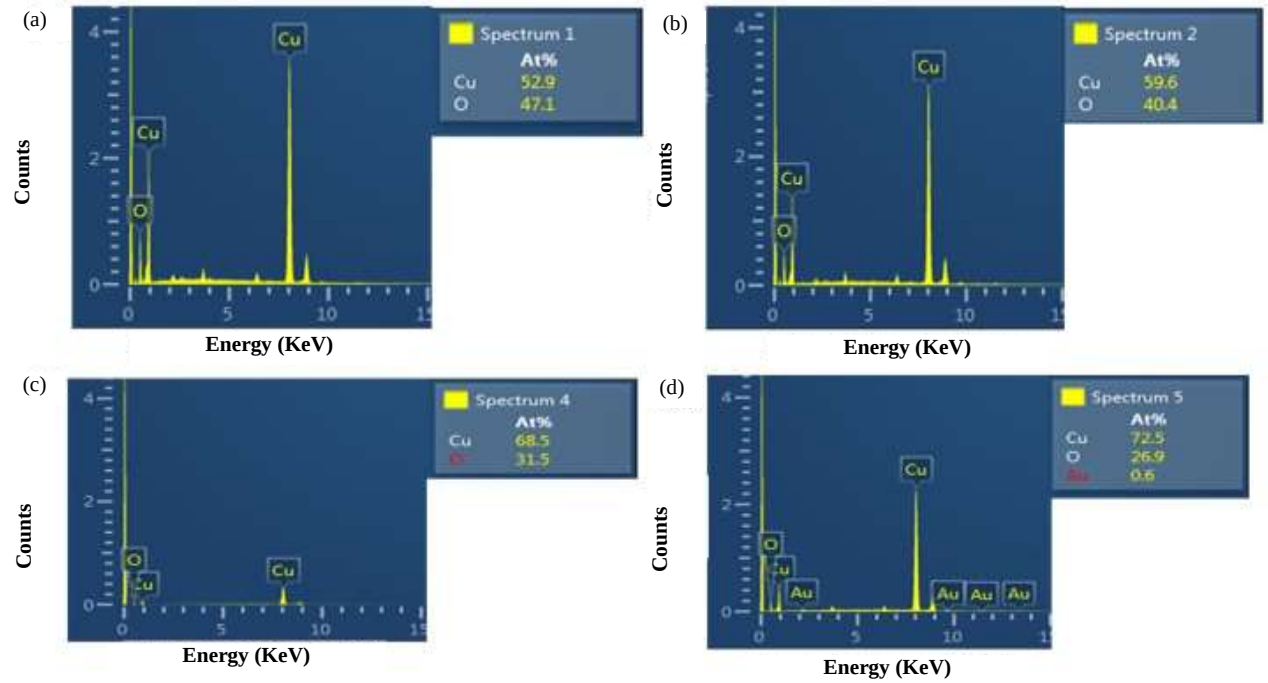

Fig. 5: EDS spectra of CuO nanomaterials treated at a different temperature, (a) as-synthesized, (b) 300 °C, (c) 500 °C, (d) 700 °C.

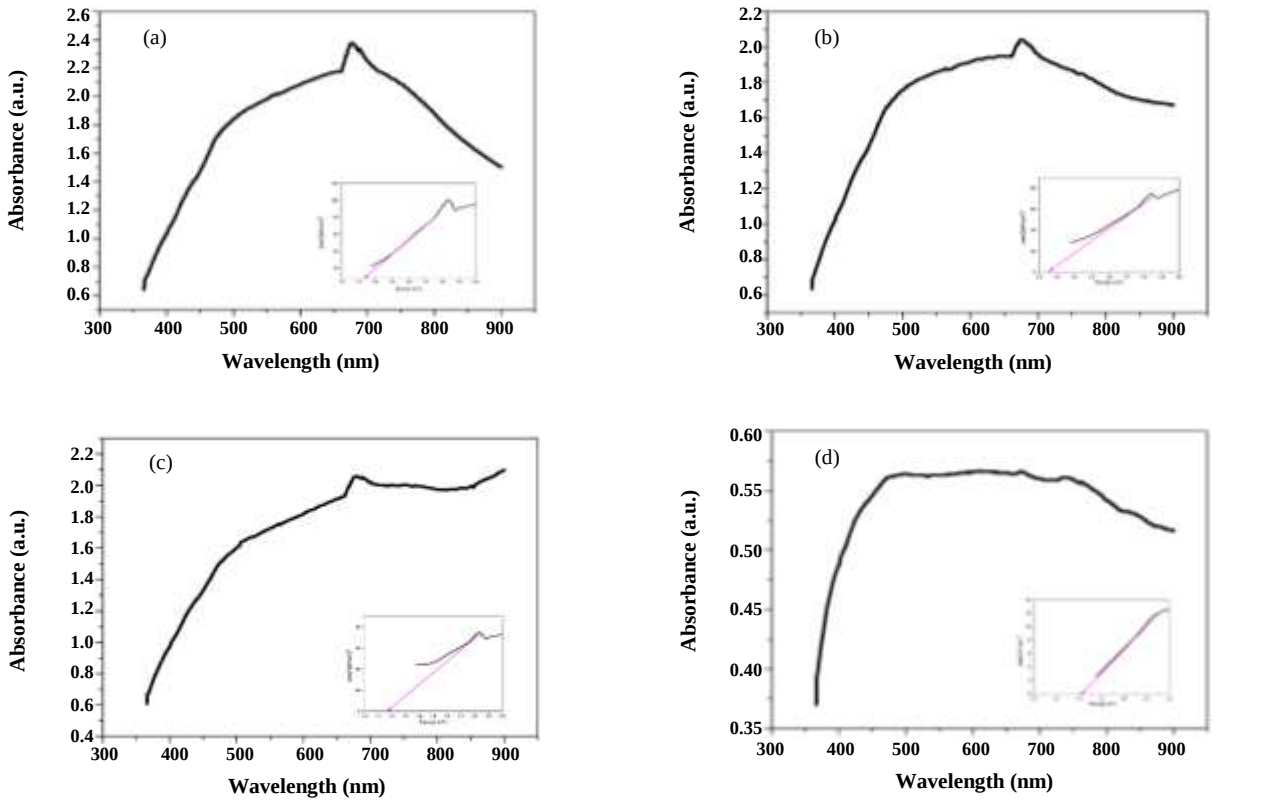

Fig. 6: UV-Visible Spectra of all the samples; (a) as-synthesized, (b) 300 °C, (c) 500 °C, (d) 700 °C. Inset: Tauc's plots of corresponding spectra for calculating the energy bandgap.

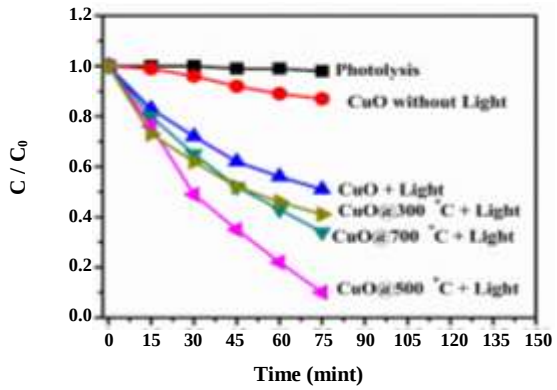

Fig. 8: Photocatalytic degradation C/C_o profile of Congo Red (CR) over CuO NPs at different time intervals.

$$ahv = A\left(hv - E_g\right)\frac{n}{2} \quad (8)$$

Where *h* is the Plank's constant, *v* is the incident photon's frequency, *α* is the absorption coefficient, *A* is a constant *n* depends on the nature of transition (*n* = 1 for direct transition), E_g is the optical energy direct bandgap [26]. and *α* is the absorption coefficient and calculated by using Eq. (9),

$$\alpha = 2.303\left(\frac{Abs}{L}\right) \quad (9)$$

Where *L* is the path length and is related to the inside width of the quartz tube. The band gap can be calculated by the intercept of a tangent on $(\alpha hv)^2$ and (hv) plots. The band gaps obtained are 1.32 eV, 1.29 eV, 1.16 eV, and 1.06 eV for the as-synthesized, 300 °C, 500 °C, and 700 °C respectively. These results are indicating that the bandgap is being reduced with the increase in temperature. *Vidyasagar et al* [14] also observed a reduction in the bandgap with the increase in annealing temperature of CuO from 400 °C to 800 °C and attributed a decrease in the bandgap to the improvement of the crystallinity of the material. Our results are also consistent, which is showing that calcination temperature is an important parameter for tuning the bandgap of the semiconductor materials.

FT-IR Analysis

FT-IR spectroscopy is a useful tool for the identification of functional groups and bonding information. Fig. 7 represents the FT-IR spectra of as-synthesized and calcinated at 300 °C, 500 °C, and 700 °C copper oxide NPs. The FTIR spectra show different well-defined absorption bands at 601.68 cm^{-1}, 774.70 cm^{-1}, 879.47 $cm^{-1,}$ and 1418.70 cm^{-1}. The occurrence of prominent peaks at 601.11 and 774.70 cm^{-1} is linked with the stretching vibrations of Metal – Oxygen (Cu – O) bonds, thereby reinforcing CuO formation [38-40]. The absorption peak at 1412 cm^{-1} can be associated with CO^{2-}, generally appearing due to sampling preparation for the FT-IR spectrum [41], whereas, the band at 1418.7 cm^{-1} belongs to in-plane OH bending [42].

Photocatalytic activity

Decolorization of textile organic dyes is an important concern in the modern industrial world. Therefore, the potential of as-prepared CuO NPs has been evaluated against the degradation of azo dye Congo Red (CR) under visible light at different time intervals. Fig. 8 exhibits the concentration change of CR dye solution at different intervals of time. For comparison purposes degradation was also observed in photolysis, CuO without light, and CuO with light. It is observed that the CR dye degraded/decompose 90 % within 75 min over CuO NPs@500 °C. The rate constants were also measured for all the samples and it is found that CuO NPs@500 °C has a high rate of degradation K = 0.08 min^{-1} than the others 0.031, 0.0468, and 0.0588 min^{-1}. The influence of catalyst dose (10, 50, 100, 200, 400 ppm) on CR dye was also investigated (Fig. 9a); and it was noticed 0.1 g/L is the optimum amount of CuO NPs to exhibit superior degradation. When the catalyst amount is small, the surface area diminishes which results in low photo decolorization of dye [43,5-7], while at a higher dose of catalyst, the degradation rate decreases because the absorption of light is restricted to the upper layer and limits scattering of the photons upon the CuO surface, consequently, did not produce sufficient light intensity for subsequent layers of the solution [44]. The effect of dye concentrations (10, 15, 20, 25, 30 ppm) was also checked by making a different amount of solution of CR dye (Fig. 9b). It is observed that degradation reduces as the dye amount increases. A large amount of dye prohibits the invasion of light into the CR layers which makes it difficult to excite the reactive state of the nanomaterials. Another perception of nominal degradation is reduced surface area availability of CuO nanomaterials which cause lesser production of hydroxyl and oxide radicals [45].

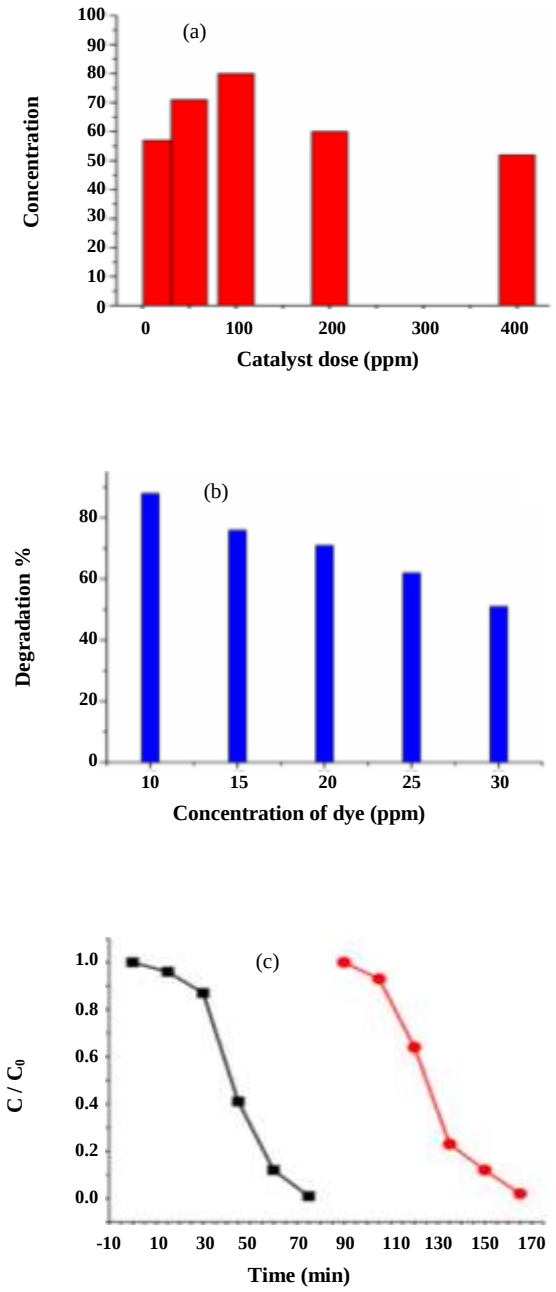

Fig. 9: Photodegradation of CR dye for different (a) CuO (10, 50, 100, 200, 400 ppm) catalyst dose (treated at 500 °C), (b) CR dye, concentration (10, 15, 20, 25, 30 ppm), (c) Recyclability, and reusability of CuO nanomaterials for CR dye solution.

For practical uses, reusability and stability are essential for cost-effectiveness. Two runs for the degradation of CR dye solution over CuO NPs were cycled. It was experimentally noticed CuO NPs exhibited good stability and recyclability as indicated in Fig. 9c.

CONCLUSIONS

In summary, crystalline CuO NPs having monoclinic structures have been prepared through the chemical co-precipitation method. The crystallinity of the samples has been improved by calcination temperature. XRD results indicate variation in parameters such as lattice parameters, volume, packing factor, and density with the temperature rise. An increase in calcination temperature also affects the growth directions. Grain and morphology also vary with the temperature rise. The optical band gap varies with the temperature and shows a minimum value at 500 °C. The photocatalytic degradation of CR dye using CuO NPs has been evaluated. It is observed that CuO nanomaterials calcinated at 500 °C are more efficient for dye degradation as compared to other calcination temperatures.

Received :May 14, 2021 ; Accepted : Aug. 16, 2021

REFERENCES

[1] Andre R.S., Sanfelice R.C., Pavinatto A., Mattoso L.H., Correa D.S., Hybrid Nanomaterials Designed for Volatile Organic Compounds Sensors: A Review, *Mater. Des.*, **156**: 154-166 (2018).

[2] Joy J., Mathew J., George S.C., Nanomaterials for Photoelectrochemical Water Splitting–Review, *Int. J. Hydrog. Energy*, **43(10)**: 4804-4817 (2018).

[3] Bogue R., Nanomaterials for Gas Sensing: A Review of Recent Research, *Sens. Rev.*, **34(1)**: 1-8 (2014).

[4] Khot L.R., Sankaran S., Maja J.M., Ehsani R., Schuster E.W., Applications of Nanomaterials in Agricultural Production and Crop Protection: A Review, *Crop Prot.*, **35**: 64-70 (2012).

[5] Sajid M.M., Amin N., Shad N.A., Javed Y., Zhang Z., Hydrothermal Fabrication of Monoclinic Bismuth Vanadate (m-$BiVO_4$) Nanoparticles for Photocatalytic Degradation of Toxic Organic Dyes, *M.S.E.B.*, **242**: 83-89 (2019).

[6] Sajid M.M., Shad N.A., Javed Y., Khan S.B., Imran Z., Hassan S., Hussain Z., Zhang Z., Amin N., Fast Surface Charge Transfer with Reduced Band Gap Energy of $FeVO_4$/Graphene Nanocomposite and Study of Its Electrochemical Property and Enhanced Photocatalytic Activity, *Arabian Journal for Science and Engineering*, **44 (7)**: 6659-6667 (2019).

[7] Shad N.A., Sajid M.M., Amin N., Javed Y., Akhtar K., Ahmad G., Hassan S., Ikram M., Photocatalytic Degradation Performance of Cadmium Tungstate (CdWO4) Nanosheets-Assembly and Their Hydrogen Storage Features, *Ceramics International*, **45(15)**: 19015-19021 (2019).

[8] Shad N.A., Sajid M.M., Haq A-U, Amin N., Imran Z., Anwar H., Ali K., Hussain Z., Younus A., Javed Y., Photocatalytic Investigation of Cadmium Oxide Nanosheets Prepared by Hydrothermal Method, *Arabian Journal for Science and Engineering*, **44(7)**: 1-7 (2019).

[9] Low F.W., Lai C.W., Recent Developments of Graphene-TiO_2 Composite Nanomaterials as Efficient Photoelectrodes in Dye-Sensitized Solar Cells: A Review, *Renewable and Sustainable Energy Reviews*, **82**:103-125 (2018).

[10] Hodges B.C., Cates E.L., Kim J-H., Challenges and Prospects of Advanced Oxidation Water Treatment Processes Using Catalytic Nanomaterials, *Nature Nanotechnology*, **13(8)**: 642-650 (2018).

[11] Sun Y., Liu N., Cui Y., Promises and Challenges of Nanomaterials for Lithium-Based Rechargeable Batteries, *Nature Energy*, **1(7)**:16071 (2016).

[12] Carpenter M.A., Mathur S., Kolmakov A., Metal Oxide Nanomaterials for Chemical Sensors, Springer Science & Business Media, (2012).

[13] Vayssieres L., On The Design of Advanced Metal Oxide Nanomaterials, *International Journal of Nanotechnology*, **1(1-2)**: 1-41 (2004).

[14] Vidyasagar C., Naik Y.A., Venkatesha T., Viswanatha R., Solid-State Synthesis and Effect of Temperature on Optical Properties of CuO Nanoparticles, *Nano-Micro Letters*, **4(2)**: 73-77 (2012).

[15] Hansen B.J., Kouklin N., Lu G., Lin I-K., Chen J., Zhang X., Transport, Analyte Detection, and Opto-Electronic Response of p-Type CuO Nanowires, *The Journal of Physical Chemistry C*, **114 (6)**: 2440-2447 (2010).

[16] Sheikholeslami M., Solidification of NEPCM under the Effect of Magnetic Field in a Porous Thermal Energy Storage Enclosure Using CuO Nanoparticles, *Journal of Molecular Liquids*, **263**:303-315 (2018).

[17] Liu X., Sun Y., Yu M., Yin Y., Du B., Tang W., Jiang T., Yang B., Cao W., Ashfold M.N., Enhanced Ethanol Sensing Properties of Ultrathin ZnO Nanosheets Decorated with CuO Nanoparticles, *Sensors and Actuators B: Chemical*, **255**: 3384-3390 (2018).

[18] Jiang T., Bujoli-Doeuff M., Gautron E., Farré Y., Cario L., Pellegrin Y., Boujtita M., Odobel F., Jobic S., Cu_2O@CuO Core-Shell Nanoparticles as Photocathode for P-Type Dye Sensitized Solar Cell, *Journal of Alloys and Compounds*, **769**: 605-610 (2018).

[19] Yuan J., Zhang J-J, Yang M-P, Meng W-J, Wang H., Lu J-X, CuO Nanoparticles Supported on TiO_2 with High Efficiency for CO_2 Electrochemical Reduction to Ethanol, *Catalysts*, **8(4)**: 171 (2018).

[20] Wang P., Gou X-X., Xin S., Cao F-F, Facile Synthesis of CuO Nanochains as High-Rate Anode Materials for Lithium-Ion Batteries, *New Journal of Chemistry*, **43(17)**: 6535-6539 (2019).

[21] Heinemann M., Eifert B., Heiliger C., Band Structure and Phase Stability of the Copper Oxides Cu_2O, CuO, and Cu_4O_3, *Physical Review B*, **87(11)**: 115111 (2013).

[22] El-Trass A., ElShamy H., El-Mehasseb I., El-Kemary M., CuO Nanoparticles: Synthesis, Characterization, Optical Properties and Interaction with Amino Acids, *Applied Surface Science*, **258(7)**: 2997-3001 (2012).

[23] Rohrer G.S., Structure and Bonding in Crystalline Materials, Cambridge University Press, (2001).

[24] Zhang Q., Zhang K., Xu D., Yang G., Huang H., Nie F., Liu C., Yang S., CuO Nanostructures: Synthesis, Characterization, Growth Mechanisms, Fundamental Properties, and Applications, *Progress in Materials Science*, **60**: 208-337 (2014).

[25] Johan M.R., Suan M.S.M., Hawari N.L., Ching H.A., Annealing Effects on the Properties of Copper Oxide Thin Films Prepared by Chemical Deposition, *Int J Electrochem Sci*, **6(12)**: 6094-6104 (2011).

[26] Raship N., Sahdan M., Adriyanto F., Nurfazliana M., Bakri A., Effect of Annealing Temperature on the Properties of Copper Oxide Films Prepared by Dip Coating Technique. In: AIP Conference Proceedings, 2017. AIP Publishing, p 030121

[27] Wongpisutpaisan N., Charoonsuk P., Vittayakorn N., Pecharapa W., Sonochemical Synthesis and Characterization of Copper Oxide Nanoparticles. *Energy Procedia*, **9**: 404-409 (2011).

[28] Zhu H., Han D., Meng Z., Wu D., Zhang C., Preparation and Thermal Conductivity of CuO Nanofluid *via* a Wet Chemical Method, *Nanoscale Research Letters*, **6(1)**: 181 (2011).

[29] Phiwdang K., Suphankij S., Mekprasart W., Pecharapa W., Synthesis of CuO Nanoparticles by Precipitation Method Using Different Precursors, *Energy Procedia*, **34**: 740-745 (2013).

[30] Khashan K.S., Sulaiman G.M., Abdulameer F.A., Synthesis and Antibacterial Activity of CuO Nanoparticles Suspension Induced by Laser Ablation in Liquid, *Arabian Journal for Science and Engineering*, **41(1)**: 301-310 (2016).

[31] Mallick P., Sahu S., Structure, Microstructure And Optical Absorption Analysis of CuO Nanoparticles Synthesized by Sol-Gel Route, *Nanoscience and Nanotechnology*, **2(3)**: 71-74 (2012).

[32] Yang C., Su X., Xiao F., Jian J., Wang J., Gas sensing Properties of CuO Nanorods Synthesized by a Microwave-Assisted Hydrothermal Method, *Sensors and Actuators B: Chemical*, **158 (1)**: 299-303 (2011).

[33] Bhaduri A., Kajal, Facile Synthesis and Characterization of Cupric Oxide (CuO) Nanoparticles: Inexpensive and Abundant Candidate for Light Harvesting. In: AIP Conference Proceedings, AIP Publishing LLC, 2093:020047 (2019).

[34] Mote V., Purushotham Y., Dole B., Williamson-Hall Analysis in Estimation of Lattice Strain in Nanometer-Sized ZnO Particles, *Journal of Theoretical and Applied Physics*, **6(1)**: 6 (2012).

[35] Marou F., Claverie A., Salles P., Martinez A., The Enhanced Diffusion of Boron in Silicon after High-Dose Implantation and During Rapid Thermal Annealing, *Nuclear Instruments and Methods in Physics Research Section B: Beam Interactions with Materials and Atoms*, **55(1-4)**: 655-660 (1991).

[36] Hu M.Z-C., Harris M.T., Byers C.H., Nucleation and Growth for Synthesis of Nanometric Zirconia Particles by Forced Hydrolysis, *Journal of Colloid and Interface Science*, **198(1)**: 87-99 (1998).

[37] Mahato T., Singh B., Srivastava A., Prasad G., Srivastava A., Ganesan K., Vijayaraghavan R., Effect of calcinations Temperature of CuO Nanoparticle on the Kinetics of Decontamination and Decontamination Products of Sulphur Mustard, *Journal of Hazardous Materials*, **192(3)**: 1890-1895 (2011).

[38] Gao X., Bao J., Pan G., Zhu H., Huang P., Wu F., Song D., Preparation and Electrochemical Performance of Polycrystalline and Single Crystalline CuO Nanorods as Anode Materials for Li Ion Battery, *The Journal of Physical Chemistry B*, **108 (18)**: 5547-5551 (2004).

[39] Kumar R.V., Mastai Y., Diamant Y., Gedanken A., Sonochemical Synthesis of Amorphous Cu and Nanocrystalline Cu_2O Embedded in a Polyaniline Matrix. Journal of Materials Chemistry, 11 (4):1209-1213 (2001).

[40] Maruyama T., Copper Oxide thin Films Prepared by Chemical Vapor Deposition from Copper Dipivaloylmethanate. *Solar Energy Materials and Solar Cells*, **56 (1)**:85-92 (1998).

[41] Kim S., Umar A., Kumar R., Ibrahim A.A., Kumar G., Facile Synthesis and Photocatalytic Activity of Cocoon-Shaped CuO Nanostructures. *Materials Letters*, **156**:138-141 (2015).

[42] Suresh S., Karthikeyan S., Jayamoorthy K., FTIR and Multivariate Analysis to Study the Effect of Bulk and Nano Copper Oxide on Peanut Plant Leaves. *Journal of Science: Advanced Materials and Devices*, **1 (3):**343-350 (2016).

[43] Anwar H., Rana B., Javed Y., Mustafa G., Ahmad M.R., Jamil Y., Akhtar H., Effect of ZnO on Photocatalytic Degradation of Rh B and Its Inhibition Activity for C. *Coli* Bacteria. Russian Journal of Applied Chemistry, 91 (1):143-149 (2018).

[44] Shad N.A., Sajid M.M., Javed Y., Ikram M., Hussain M.I., Nawaz S., Afzal A.M., Hussain S.Z., Amin N., Yousuf I., Lamellar Shape Lead Tungstate (PbWO4) Nanostructures as Synergistic Catalyst for Peroxidase Mimetic Activity. *Materials Research Express*, **7**: 015520 (2020).

[45] Kumar M., Das R.R., Samal M., Yun K., Highly Stable Functionalized Cuprous Oxide Nanoparticles for Photocatalytic Degradation of Methylene Blue. *Materials Chemistry and Physics*, **218**:272-278 (2018).